Nano Research 2015, 8(9): 3020–3026
DOI 10.1007/s12274-015-0807-x
Research Article

ISSN 1998-0124
CN 11-5974/O4

Hole-doping of mechanically exfoliated graphene by confined hydration layers

Tjeerd R. J. Bollmann[1,2] (✉), Liubov Yu. Antipina[3,4], Matthias Temmen[2], Michael Reichling[2], and Pavel B. Sorokin[5]

[1] *Inorganic Materials Science, MESA+ Institute for Nanotechnology, P. O. Box 217, 7500AE Enschede, The Netherlands*
[2] *Fachbereich Physik, Universität Osnabrück, Barbarastraße 7, Osnabrück 49076, Germany*
[3] *Moscow Institute of Physics and Technology, Dolgoprudny 141700, Russian Federation*
[4] *Siberian Federal University, Krasnoyarsk 660041, Russian Federation*
[5] *National University of Science and Technology MISiS, Moscow 119049, Russian Federation*

Received: 19 February 2015
Revised: 22 April 2015
Accepted: 28 April 2015

KEYWORDS

graphene,
non-contact atomic force microscopy (NC-AFM, KPFM),
liquid–solid interface structure,
electronic transport in nanoscale materials and structures

ABSTRACT

By the use of non-contact atomic force microscopy (NC-AFM) and Kelvin probe force microscopy (KPFM), we measure the local surface potential of mechanically exfoliated graphene on the prototypical insulating hydrophilic substrate of CaF_2(111). Hydration layers confined between the graphene and the CaF_2 substrate, resulting from the graphene's preparation under ambient conditions on the hydrophilic substrate surface, are found to electronically modify the graphene as the material's electron density transfers from graphene to the hydration layer. Density functional theory (DFT) calculations predict that the first 2 to 3 water layers adjacent to the graphene hole-dope the graphene by several percent of a unit charge per unit cell.

1 Introduction

The demonstration of the two-dimensional electronic properties of mechanically exfoliated graphene [1] has increased interest in investigating the unique properties of both graphene and other 2D materials. In comparison to other preparation methods, the mechanical exfoliation of graphene on a substrate results in flakes of high quality [1, 2]. The ambient conditions during this method of preparation, however, affect the electronic properties of 2D materials [3] in uncontrolled manners. This results from the capture of thin water layers from moisture present in the atmosphere [4–12]. Confined water layers have been

Address correspondence to tbollman@uos.de

described as modifying the electronic properties of the graphene, as they are thought to effectively shield the interfacial charge on electrically insulating substrates [10]. A negative surface charge has been reported for "electroneutral" mica substrates; this was understood to be caused by the confined water layer, which has been suggested to have the potential to dope the graphene. The mechanism of electronic modification by confined water between the substrate and exfoliated graphene, however, is not yet well-understood [10, 13].

Here, we study the electronic properties of mechanically exfoliated graphene containing confined hydration layers (HLs) that result from the preparation of graphene under ambient conditions on a prototypical insulating hydrophilic substrate of CaF_2(111). Using non-contact atomic force microscopy (NC-AFM) and Kelvin probe force microscopy (KPFM), we investigate changes in the surface potential induced by the partial removal of HLs upon heating. To investigate the origin of the electronic modification of graphene by HLs of different thicknesses, we compare experimentally obtained topography and KPFM measurements to a quantitative model calculated by density functional theory (DFT). Our observations demonstrate the role of charge transfer between the HLs and graphene in the modification of the graphene's electronic properties.

2 Experimental

Graphene was mechanically exfoliated [1] under ambient conditions from a highly ordered pyrolytic graphite (HOPG) crystal onto a CaF_2(111) substrate, which had been cleaved under similar conditions a short time before [12]. The resulting graphene flakes were inspected by optical microscopy before their insertion into an ultra-high vacuum chamber (UHV). To indicate the graphene flakes' thickness in general, we characterized the thickness of the graphene flakes beyond the available optical spot size by Raman microscopy, using the G and 2D bands [14, 15]. Prior to the NC-AFM measurements, the sample was heated under UHV conditions with a base pressure below 1×10^{-10} mbar to 400 K to partially remove the thicker HLs by dehydration [12]. NC-AFM measurements were performed with a well- characterized system [16–18] in which KPFM [19, 20] measurements were performed simultaneously by applying an AC voltage of 1 V_{PP} amplitude and a frequency of 1.2 kHz, in addition to the DC bias regulated to minimize electrostatic forces. In KPFM measurements, the measured potential is relative to the reference potential, which is defined here as the tip potential. By recording the NC-AFM and KPFM images simultaneously, we obtained correct height information and identified different graphene sheet thicknesses [12] in a controlled UHV environment beyond the spatial resolution attainable by (micro-) Raman spectroscopy, without the risk of heating or even boiling the confined HLs by laser irradiation [21].

The simulation calculations were performed using DFT [22, 23] within the generalized gradient approximation (GGA) of the Perdew-Burke-Ernzerhof [24] parametrization with periodic boundary conditions using the Vienna *Ab-initio* Simulation Package [25–27]. The projector augmented-wave (PAW) method was used, along with a plane-wave basis set with an energy cutoff at 425 eV. To calculate atomic and electronic structures, the Brillouin zone was sampled according to the Monkhorst-Pack [28] scheme with 4 × 4 *k*-points in periodical directions, combining the graphene 3 × 3 and CaF_2(111) 2 × 2 super-cells with lattice constants of $a_{graphene} = 2.46$ Å and $a_{CaF_2(111)} = 3.86$ Å. To avoid spurious interactions between neighboring structures in the tetragonal super-cell, a vacuum layer of 17 Å was included in all non-periodic directions. The water density was set to 8.43 water molecules per nm^2, which is slightly below the density of liquid water but in agreement with literature values [29, 30]. Structural relaxation was performed until the forces acting on each atom were less than 0.05 eV/Å. Molecular dynamics (MD) simulations were performed at 300 K using the Nosè-Hoover thermostat [31, 32] over 10 ps with time steps of 1 fs. For analysis of the atomic geometry and electronic properties, statistics were taken from 10 snapshots randomly chosen after equilibrium was established for all situations investigated, which are described below.

3 Results

To visualize the changes in the electronic properties of graphene, we imaged the graphene flakes' topography by NC-AFM and the corresponding surface potential by KPFM, as shown in Fig. 1. A triple layer of F^--Ca^{2+}-F^-

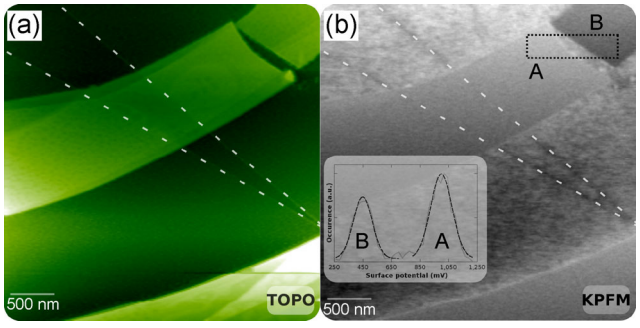

Figure 1 (color on-line) Topography (a) and local surface potential (b) image of few-layer graphene flakes. Substrate steps are marked by (white) dashed lines in both (a) and (b). Graphene flakes A and B, located near each other, show strong differences in their local surface potentials; the inset shows a fit of normal distributions to the local surface potential values found in the area enclosed by the dashed rectangle.

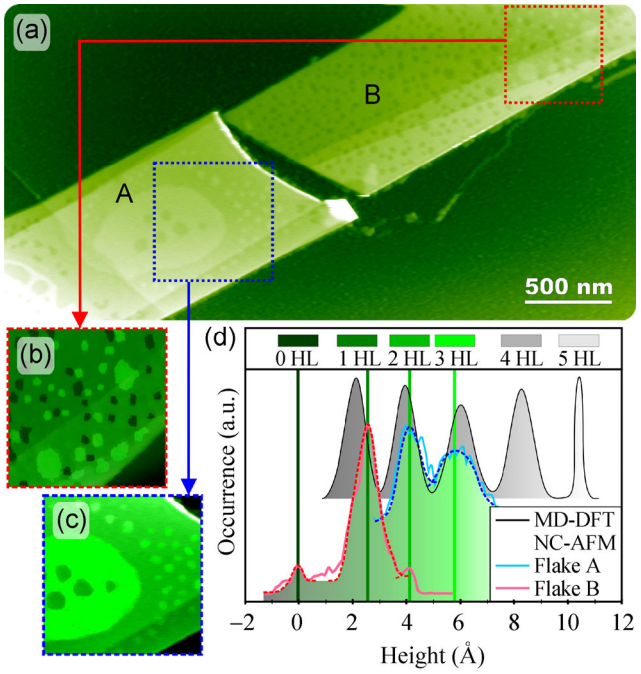

Figure 2 (color on-line) NC-AFM image (a) of two few-layer graphene flakes, corresponding to flakes labeled A and B in Fig. 1. From the height histograms of the Kuwahara-filtered [34] areas marked in the corresponding red (b) and blue (c), the height levels of the first three HLs (d) are identified. Experimental data is fitted by normal distributions and color-coded corresponding to images (b) and (c). Height levels marked in gray are obtained from DFT calculations.

substrate steps can be identified in both the topographic and KPFM images [33]. The contrast observed between the few-layer graphene flakes labeled A and B in Fig. 1(b), which are of similar heights, cannot be ascribed to differences in their thicknesses (approximately five layers), as KFPM images can only distinguish one, two, and three layers of graphene with reasonable contrast [12]. Notably, the contrast distinguishing the thinnest graphene sheets from each other is equivalent to ~110 mV [12, 35], while the surface potential of flake B is 550 mV lower than that of flake A.

To investigate the mechanism responsible for this strong contrast, we investigated the topography of flakes A and B in detail, as shown in Fig. 2(a). Mild annealing of the graphene and its confined water layers at 400 K results in a decay of HLs [12] and changes in the height levels for the flakes shown in Fig. 2(a). By plotting the height distributions of the corresponding dashed rectangles (Figs. 2(b)–2(c)) in Fig. 2(d), we can determine the heights of the individual HLs. Graphene flake A confines a full second HL and part of a third HL; flake B confines the majority of a first HL, with areal coverage of 80% ± 2%, with some second HL patches as seen in the top right corner of Fig. 2(a). To understand the dependence of the surface potential on the number of HLs confined between the graphene and substrate, we performed MD simulations of the system at room temperature (300 K) in which the number of confined HLs was varied from zero to five. Results of the simulation, shown in Figs. 2(d) and 3, reveal the heights of the HLs as determined from the distance between graphene and substrate, in agreement with our experimental observations as evident from Fig. 2(d). We can obtain the simulated difference in charge density between the electronic density of the calculated structure as a whole, as depicted in Fig. 3, and the summation of the electronic density of free-standing graphene and freestanding slabs of CaF_2(111) with that of HLs present on top. This comparison allows us to directly see the redistribution of charge originating from the interaction between the HLs and the graphene. As clearly seen in Fig. 3, in the first 2–3 HLs right below the graphene layer, water molecules orient to create a net dipole, which draws the graphene's electrons slightly towards the adjacent HL. Apart from a minor charge redistribution on the upper fluorite layer, the strongly ionic CaF_2 substrate makes no significant contribution to graphene's electronic properties. Therefore, we conclude that the confined water layers do not only shield the interfacial charge at

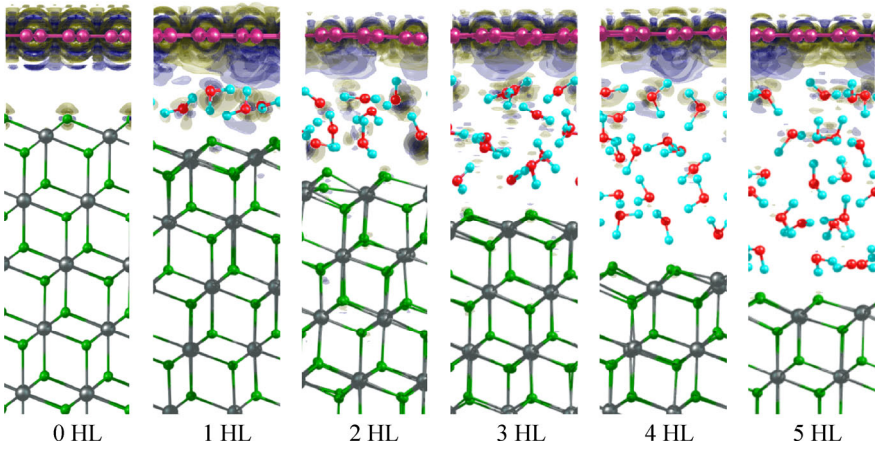

Figure 3 (color on-line) MD snapshots of the atomic positions for n HLs confined by graphene and the $CaF_2(111)$ substrate underneath (side view), with the electronic influx and outflux marked in blue and yellow, respectively. The calculated electronic redistribution reveals the net dipole formation of the first three HLs below the graphene. Carbon (violet), oxygen (red), hydrogen (cyan), calcium (gray), and fluorine (green) atoms are marked.

the substrate [10], but also contribute to the graphene's electronic rearrangement, while the substrate remains "electroneutral". The electronic contribution of the confined HLs to the graphene above is determined by a Bader analysis [36] of the charge distribution, with results summarized in Fig. 4. In this figure, the reduction in free charge carrier density per unit cell (uc) is graphed for increasing numbers of HLs. When no HLs are present, we define the free charge carrier density of graphene as zero. From this analysis, we find a decrease in electron density, and a corresponding increase in hole density, for graphene as the number of HLs increases. As the free charge carrier density within graphene decreases under the influence of the highly electronegative oxygen atoms in the water molecules, which attract electron density, the confined HLs effectively create hole-doped graphene. This conclusion is in agreement with the observation of increasing surface potential, as indicated by brighter contrast, for decreasing graphene thickness, as represented in Fig. 1(d) of Ref. [12]. Since we can determine from Fig. 3 that only the 2 to 3 HLs adjacent to the graphene contribute to its electronic rearrangement, we expect asymptotic behavior for electron transfer as a function of the number of confined HLs, which is well in accordance with the DFT results shown in Fig. 4.

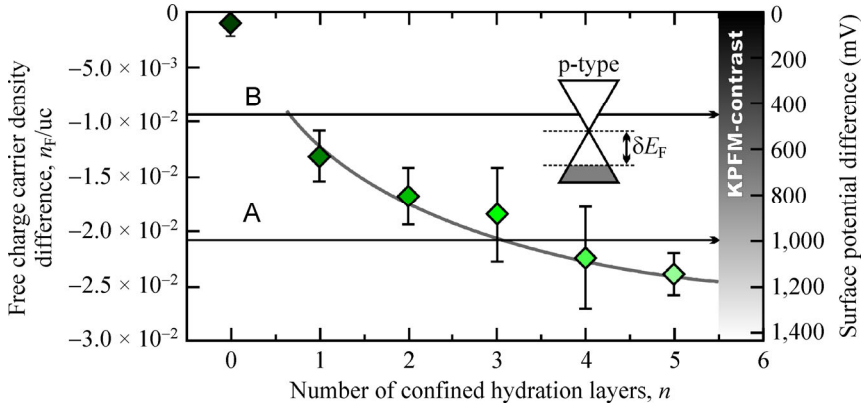

Figure 4 The decaying free charge carrier density of graphene for increasing numbers of confined HLs, representing the increase of holes for greater numbers of confined HLs. The gray line serves as a guide-to-the-eye for the asymptotic behavior of charge carrier density in response to thick confined HLs. The calculated surface potential difference and corresponding contrast in KPFM imaging is shown at the right.

4 Discussion

Because of the strong delocalization of electrons in graphene, the homogeneous contrast in our KPFM measurements reflects the decrease in electron density for increased numbers of confined HLs, which represents the more positive charge of hole-doped graphene. The contrast of 550 mV between graphene flakes A and B in Fig. 1 quantitatively demonstrates the lower electron density of flake A compared to flake B. This decrease in electron density arises from the thicker confined HLs present, measured at approximately 2.5 ML of flake A from the topographic image in Fig. 2(a). The less decreased electron density for flake B, meanwhile, as revealed by the more negative surface potential observed by KPFM, arises from the smaller average thickness and the partial absence (20%) of HLs.

To quantitatively compare the doping observed in our experiments to the calculated free charge carrier density plotted in Fig. 4, we used a simple capacitor model [37]. This choice was based on the approximation of graphene's density of states (DOS) as linear within the vicinity of the conical points [38], since the interaction between HLs and graphene is weak; details of the graphene's band structure near the K-point for few layer graphene (FLG) [39] do not affect the Fermi level shifts discussed here. Notably, in our experimental setup, the potential difference between the tip and the backside electrode of the insulating substrate was measured; for the system under investigation, this measurement is effectively dominated by the potential difference across the substrate and HL. The determined surface potential difference corresponds to a Fermi level shift [38] in the graphene flake, proportional to the density of free charge carriers at the Fermi-level (n_F) as:

$$\Delta n_F = \left(\frac{\delta E_F}{\hbar v_F} \right)^2 / \pi$$

where δE_F is the Fermi level shift and the Fermi velocity $\hbar v_F$ is equal to 6.726 eVÅ [40, 41]. Assuming the Fermi level shift of 550 mV, as determined between flakes A and B in Fig. 1(b), we can determine an increase in free charge carrier density of 2.1×10^{-3} carriers per Å^2. Applying the uc area of graphene (5.24 Å^2), this translates to 0.011 holes/uc. This is similar to the value expected by extrapolating the free charge carrier density and corresponding surface potential difference as calculated in the graph shown in Fig. 4, from which we estimated the average HL coverage as 0.8 ML and 2.5 ML in the analysis discussed above. For an accurate estimate of the free charge carrier density, one should take the average coverage of the entire flake into account, as well as the screening of the electrical field for larger numbers of graphene layers [42]. Our simple model predicts that the surface potential between a system without confined HLs in comparison to a system with one HL present is one order of magnitude larger than the decrease in surface potential for incrementing the number of confined HLs present, which agrees with experimental observations of confined water layers on mica [10]. The different HL heights present under the same flake do not correlate to the KPFM image data, although the resolution in KPFM is demonstrated to be several tens of mV by our ability to discriminate the CaF_2(111) substrate ledges in KPFM [33] in Fig. 1(b). This uniform doping over the entire flake, however, can be easily understood as arising from the free delocalized electrons present in graphene. In contrast to graphene on mica [10, 13], we observe no local doping, where the edges of the water-free domains [12] might serve as demarcations for variations in doping levels. This might result from the materials' different behavior upon cleavage, which leaves more charge on the surface of mica than it does on CaF_2(111).

5 Summary

We elucidated the processes of the hole-doping of graphene by confined HLs by imaging the topography of HLs by NC-AFM and correlating this with surface potential data obtained by KPFM. The HLs confined upon mechanical exfoliation not only influence the mechanical properties of graphene [12], but also contribute to the hole-doping of graphene. By comparing the experimentally determined surface topography with MD-DFT calculations, we identified different HLs and described their electronic contribution to the graphene. The 2 to 3 HLs adjacent to the graphene were found to cause the hole-doping of graphene by forming a net dipole which draws the graphene's

electrons slightly towards the HLs. HLs beyond this thickness or depth only marginally contribute to hole doping. Although this investigation was performed specifically on a CaF_2(111) substrate, its findings can be generalized, as the hydrophilic substrate does not affect the electronic rearrangement. This doping mechanism could be induced in a controlled manner by creating specific hydrophobic/hydrophilic substrate architectures, among other methods, which would tailor graphene's electronic properties for use in future applications such as humidity sensors.

Acknowledgements

This work was supported by the SPP 1459 of the Deutsche Forschungsgemeinschaft. We thank O. Ochedowski for help in sample preparation. M. T. gratefully appreciates support from the Hans Mühlenhoff-Stiftung. We are grateful to the "Chebishev" and "Lomonosov" supercomputers of Moscow State University and the Joint Supercomputer Center of the Russian Academy of Sciences for the possibility of using a cluster computer for quantum-chemical calculations. P. B. S. gratefully acknowledges the financial support of the Ministry of Education and Science of the Russian Federation in the framework of the Increase Competitiveness Program of NUST «MISiS» (No. K2-2015-033). L. Y. A. acknowledges the support from the Russian Science Foundation (No. 14-13-00139).

References

[1] Novoselov, K. S.; Geim, A. K.; Morozov, S. V.; Jiang, D.; Zhang, Y.; Dubonos, S. V.; Grigorieva, I. V.; Firsov, A. A. Electric field effect in atomically thin carbon films. *Science* **2004**, *306*, 666–669.

[2] Tang, D.-M.; Kvashnin, D. G.; Najmaei, S.; Bando, Y.; Kimoto, K.; Koskinen, P.; Ajayan, P. M.; Yakobson, B. S.; Sorokin, P. B.; Lou, J. et al. Nanomechanical cleavage of molybdenum disulphide atomic layers. *Nat Commun.* **2014**, *5*, 3631.

[3] Song, J.; Ko, T. Y.; Ryu, S. Raman spectroscopy study of annealing-induced effects on graphene prepared by micro-mechanical exfoliation. *Bull Korean Chem Soc* **2010**, *31*, 2679–2682.

[4] Xu, K.; Cao, P. G.; Heath, J. R. Graphene visualizes the first water adlayers on mica at ambient conditions. *Science* **2010**, *329*, 1188–1191.

[5] Cao, P. G.; Xu, K.; Varghese, J. O.; Heath, J. R. The microscopic structure of adsorbed water on hydrophobic surfaces under ambient conditions. *Nano Lett* **2011**, *11*, 5581–5586.

[6] He, K. T.; Wood, J. D.; Doidge, G. P.; Pop, E.; Lyding, J. W. Scanning tunneling microscopy study and nanomanipulation of graphene-coated water on mica. *Nano Lett* **2012**, *12*, 2665–2672.

[7] Komurasaki, H.; Tsukamoto, T.; Yamazaki, K.; Ogino, T. Layered structures of interfacial water and their effects on Raman spectra in graphene-on-sapphire systems. *J. Phys. Chem. C* **2012**, *116*, 10084–10089.

[8] Lee, M. J.; Choi, J. S.; Kim, J.-S.; Byun, I.-S.; Lee, D. H.; Ryu, S.; Lee, C.; Park, B. H. Characteristics and effects of diffused water between graphene and a SiO_2 substrate. *Nano Res.* **2012**, *5*, 710–717.

[9] Severin, N.; Lange, P.; Sokolov, I. M.; Rabe, J. P. Reversible dewetting of a molecularly thin fluid water film in a soft graphene/mica slit pore. *Nano Lett.* **2012**, *12*, 774–779.

[10] Shim, J.; Lui, C. H.; Ko, T. Y.; Yu, Y.-J.; Kim, P.; Heinz, T. F. Water-gated charge doping of graphene induced by mica substrates. *Nano Lett.* **2012**, *12*, 648–654.

[11] Verdaguer, A.; Sequra, J. J.; López-Mir, L.; Sauthier, G.; Fraxedas, J. Communication: Growing room temperature ice with graphene. *J. Chem. Phys.* **2013**, *138*, 121101.

[12] Temmen, M.; Ochedowski, O.; Schleberger, M.; Reichling, M.; Bollmann. T. R. J. Hydration layers trapped between graphene and a hydrophilic substrate. *New J. Phys.* **2014**, *16*, 053039.

[13] Goncher, S. J.; Zhao, L. Y.; Pasupathy, A. N.; Flynn, G. W. Substrate level control of the local doping in graphene. *Nano Lett.* **2013**, *13*, 1386–1392.

[14] Malard, L. M.; Pimenta, M. A.; Dresselhaus, G.; Dresselhaus, M. S. Raman spectroscopy in graphene. *Phys. Rep.* **2009**, *473*, 51–87.

[15] Ferrari, A. C.; Basko, D. M. Raman spectroscopy as a versatile tool for studying the properties of graphene. *Nat. Nanotechnol.* **2013**, *8*, 235–246.

[16] Lübbe, J.; Tröger, L.; Torbrügge, S.; Bechstein, R.; Richter, C.; Kühnle, A.; Reichling, M. Achieving high effective Q-factors in ultra-high vacuum dynamic force microscopy. *Meas. Sci. Technol.* **2010**, *21*, 125501.

[17] Lübbe, J.; Doering, L.; Reichling, M. Precise determination of force microscopy cantilever stiffness from dimensions and eigenfrequencies. *Meas. Sci. Technol.* **2012**, *23*, 045401.

[18] Lübbe, J.; Temmen, M.; Rode, S.; Rahe, P.; Kühnle, A.; Reichling, M. Thermal noise limit for ultra-high vacuum noncontact atomic force microscopy. *Beilstein J. Nanotechnol.* **2013**, *4*, 32–44.

[19] Nonnenmacher, M.; O'Boyle, M. P.; Wickramasinghe, H. K. Kelvin probe force microscopy. *Appl. Phys. Lett.* **1991**, *58*, 2921–2923.

[20] Weaver, J. M. R.; Abraham, D. W. High resolution atomic force microscopy potentiometry. *J. Vac. Sci. Technol. B* **1991**, *9*, 1559–1561.

[21] Frolov, V. D.; Pivovarov, P. A.; Zavedeev, E. V.; Khomich, A. A.; Grigorenko, A. N.; Konov, V. I. Laser-induced local profile transformation of multilayered graphene on a substrate. *Opt. Laser Technol.* **2015**, 69, 34–38.

[22] Hohenberg, P.; Kohn, W. Inhomogeneous electron gas. *Phys. Rev.* **1964**, *136*, B864–B871.

[23] Kohn, W.; Sham, L. J. Self-consistent equations including exchange and correlation effects. *Phys. Rev.* **1965**, *140*, A1133–A1138.

[24] Perdew, J. P.; Burke, K.; Ernzerhof, M. Generalized gradient approximation made simple. *Phys. Rev. Lett.* **1996**, *77*, 3865–3868.

[25] Kresse, G.; Hafner, J. Ab initio molecular dynamics for liquid metals. *Phys. Rev. B* **1993**, *47*, 558–561.

[26] Kresse, G.; Hafner, J. Ab initio molecular-dynamics simulation of the liquid-metal-amorphous-semiconductor transition in germanium. *Phys. Rev. B* **1994**, *49*, 14251–14269.

[27] Kresse, G.; Furthermüller, J. Efficient iterative schemes for ab initio total-energy calculations using a plane-wave basis set. *Phys. Rev. B* **1996**, *54*, 11169–11186.

[28] Monkhorst, H. J.; Pack, J. D. Special points for Brillouin-zone integrations. *Phys. Rev. B* **1976**, *13*, 5188–5192.

[29] Reischl, B.; Watkins, M.; Foster, A. S. Free energy approaches for modeling atomic force microscopy in liquids. *J. Chem. Theory Comput.* **2013**, *9*, 600–608.

[30] Moser, J.; Verdaguer, A.; Jiménez, D.; Barreiro, A.; Bachtold, A. The environment of graphene probed by electrostatic force microscopy. *Appl. Phys. Lett.* **2008**, *92*, 123507.

[31] Nosè, S. A unified formulation of the constant temperature molecular dynamics methods. *J. Chem. Phys.* **1984**, *81*, 511–519.

[32] Hoover, W. G. Canonical dynamics: Equilibrium phase-space distributions. *Phys. Rev. A* **1985**, *31*, 1695–1697.

[33] Pieper, H. H.; Barth, C.; Reichling, M. Characterization of atomic step structures on CaF_2(111) by their electric potential. *Appl. Phys. Lett.* **2012**, *101*, 051601.

[34] Filleter, T.; Emtsev, K. V.; Seyller, T.; Bennewitz, R. Local work function measurements of epitaxial graphene. *Appl. Phys. Lett.* **2008**, *93*, 133117.

[35] Russ, J. C. *The Image Processing Handbook (5th Ed.)*; CRC Press: Boca Raton, 2006.

[36] Bader, R. F. W. Atoms in molecules. In *Encyclopedia of Computational Chemistry*. von Ragué Schleyer, P., Ed.; Wiley: New York, 1990.

[37] Wang, F.; Zhang, Y. B.; Tian, C. S.; Girit, C.; Zettl, A.; Crommie, M.; Shen, Y. G. Gate-variable optical transitions in graphene. *Science* **2008**, *320*, 206–209.

[38] Giovannetti, G.; Khomyakov, P. A.; Brocks, G.; Karpan, V. M.; van der Brink, J.; Kelly, P. J. Doping graphene with metal contacts. *Phys. Rev. Lett.* **2008**, *101*, 026803.

[39] Latil, S.; Henrard, L. Charge carriers in few-layer graphene films. *Phys. Rev. Lett.* **2006**, *97*, 036803.

[40] Geim, A. K.; Novoselov, K. S. The rise of graphene. *Nat. Mater.* **2007**, *6*, 183–191.

[41] Bostwick, A.; Ohta, T.; Seyller, T.; Horn, K.; Rotenberg, E. Quasiparticle dynamics in graphene. *Nat. Phys.* **2007**, *3*, 36–40.

[42] Ziegler, D.; Gava, P.; Güttinger, J.; Molitor, F.; Wirtz, L.; Lazzeri, M.; Saitta, A. M.; Stemmer, A.; Mauri, F.; Stampfer, C. Variations in the work function of doped single- and few-layer graphene assessed by Kelvin probe force microscopy and density functional theory. *Phys. Rev. B* **2011**, *83*, 235434.